

Performance analysis of opto-mechatronic image stabilization for a compact space camera

K. Janschek, V. Tchernykh, S. Dyblenko*

Department of Electrical Engineering and Information Technology, Institute of Automation, Technische Universität Dresden, D-01062 Dresden, Germany

Received 25 April 2005; accepted 1 February 2006

Available online 22 March 2006

Abstract

The paper presents new performance results for the enhanced concept of an opto-mechatronic camera stabilization assembly consisting of a high-speed onboard optical processor for real-time image motion measurement and a 2-axis piezo-drive assembly for high precision positioning of the focal plane assembly. The proposed visual servoing concept allows minimizing the size of the optics and the sensitivity to attitude disturbances. The image motion measurement is based on 2D spatial correlation of sequential images recorded from an in situ motion matrix sensor in the focal plane of the camera. The demanding computational requirements for the real-time 2D-correlation are covered by an embedded optical correlation processor (joint transform type). The paper presents briefly the system concept and fundamental working principles and it focuses on a detailed performance and error analysis of the image motion tracking subsystem. Simulation results of the end-to-end image motion compensation performance and first functional hardware-in-the-loop test results conclude the paper.

© 2006 Elsevier Ltd. All rights reserved.

Keywords: Opto-mechatronics; Optical correlator; Image motion tracking; Image motion compensation; Visual servoing

1. Introduction

Size and mass of high resolution satellite cameras are usually determined by the optics. The main problems, associated with minimizing the optics size, are the degradation of the modulation transfer function (MTF), resulting in image smoothing, and darkening of the image. MTF degradation can be compensated to some extent by inverse filtering, but this can be done only at the expense of noise amplification, so a high initial signal-to-noise ratio (SNR) is required. With compact high resolution optics, however, a high SNR can be obtained only with a very long exposure time, as the focal plane image is very dark. This requires precise image motion compensation during the long exposure interval.

Image shift due to orbital motion is conventionally being compensated by time-delayed integration (TDI) which performs a corresponding shifting of the accumulated

charge packages by a special TDI-capable image sensor (Brodsky, 1992). TDI sensors have a number of disadvantages (larger pixels, additional image blurring, etc.) and do not compensate the attitude instability. This problem is currently being solved by high precision satellite attitude control systems (Salaün, Chamontin, Moreau, & Hameury, 2002; Dial & Grodecki, 2002) and by enlarging the optics aperture (to reduce the exposure time). Both solutions increase however significantly the mission cost.

To keep compact camera sizes together with small aperture optics and moderate satellite attitude stability requirements, it would be rather straightforward to use imaging systems with long exposure time and some image stabilization mechanisms to prevent from image motion distortions.

Such solutions can use one of the following stabilization principles:

- (a) Digital image correction: the camera motion is estimated from the digital input images captured by the camera and the movement correction is performed by digital processing of the camera images.

*Corresponding author. Tel.: +49 351 463 32134;
fax: +49 351 463 37039.

E-mail address: dyblenko@ifa.et.tu-dresden.de (S. Dyblenko).

- (b) Sensor based image correction: the camera motion is assessed with an external motion sensor and the movement correction is performed by digital processing of the camera images.
- (c) Opto-mechatronic stabilization: the camera motion is compensated by a mechanically driven optical system.

The most elegant solution is the full digital image correction (a), which is used in consumer video cameras (Uomori, Morimura, Ishii, Sakaguchi, & Kitamura, 1990) and video coding algorithms (Engelsberg & Schmidt, 1999). The first group deals only with compensation of certain types of translational image motion at rather low accuracy. The latter group uses more sophisticated algorithms, which can remove full first-order (affine) deformations between images in a sequence and assemble these aligned images within a single reference coordinate system to produce an image mosaic. The advanced algorithms applied, such as pyramid-based motion estimation and image warping (Hansen, Anandan, Dana, van der Wal, & Burt, 1994) or fuzzy adaptive Kalman filtering (Gullu & Erturk, 2003), allow even subpixel accuracy, but require advanced processing hardware.

The sensor-based image correction (b) suffers from the fact, that the motion sensor is normally non-located with the actual image sensor. Therefore any mechanical distortions (misalignment, structural deformations, vibration) result in image motion measurement errors, which affect the final quality of the corrected image.

The opto-mechatronic stabilization (c) is the most versatile one, because it can cope with large motion amplitudes and can make use of all benefits of the digital corrections.

The principles applied here, are very similar to the well known visual servoing (Hutchinson, Hager, & Corke, 1996). Visual servoing classically means the task to use visual information to control the pose of a robot's end-effector relative to a target object or a set of target features. Mapped onto a remote sensing camera, this task can be equivalently described as using visual information from an image sensor to control the motion of this image sensor relative to the scene to be observed.

A wide variety of visual servoing applications has been developed so far in macro-robotics (Oh & Allen, 2001) as well as in micro- and nano-robotics. In particular the latter class has strong commonalities with remote sensing camera design in term of micro- and sub-micrometer accuracies and the actuation principles applied, e.g. MEMS micro-assembly (Ralis, Vikramaditya, & Nelson, 2000; Weber & Hollis, 1989).

For visual servoing in general and opto-mechatronic stabilization in particular two tasks are of essential importance: (a) visual motion estimation & tracking and (b) pointing control.

Motion estimation is the problem of extracting the two-dimensional (2D) projection of the 3D relative motion into the image plane in the form of a field of correspondences

(motion vectors) between points in consecutive frames. For practical applications a block or window based approach has been proved to be most appropriate. The spatial dynamics of image windows is being analyzed by feature or area based methods, to derive image motion information. Feature-based methods basically use computationally efficient edge detection techniques, but they rely on structured environment with specific patterns (Hutchinson et al., 1996).

Area based methods have been proved to be much more robust in particular for image data representing unstructured environment. They exploit the temporal consistency over a series of images, i.e. the appearance of a small region in an image sequence changes little. Block matching algorithms measure the motion of a block of pixels in consecutive images, such as the sum of squared differences (SSD) algorithm, which needs to solve a minimization problem with the desired image shift vector as optimization variable (Hutchinson et al., 1996; Oh & Allen, 2001), or to apply the method of direction of minimum distortion (DMD) (Haworth, Peacock, & Renshaw, 2001; Jain & Jain, 1981).

The classical and most widely used approach is the area correlation, used originally for image registration (Pratt, 1974). Area correlation uses the fundamental property of the cross-correlation function of two images, that the location of the correlation peak gives directly the displacement vector of the image shift. Different correlation schemes are known besides the standard cross correlation, e.g. phase correlation (Weber & Hollis, 1989) or the Joint Transform Correlation (Jutamulia, 1992).

A more recent and evolving application area is the video coding (e.g. MPEG-standard) where sub-pixel accuracy is required and multiple moving area blocks have to be tracked using adaptive correlation techniques (Xu, Po, & Cheung, 1999) as well as hierarchical multi-resolution algorithms based on complex wavelets (Magarey & Kingsbury, 1998).

The limitation of the applicability of area-based methods comes from the trade-off between computational effort, robustness to non-structured image texture and signal-to-noise ratio.

The higher robustness of area based methods to weakly structured image texture and small signal-to-noise ratio (this is valid in particular for correlation-based methods) has to be paid by a considerable high computational effort. As the complete image area content has to be processed at pixel level, the real-time application is restricted to rather small image blocks in the range 8×8 to 32×32 pixels. This limits the accuracy, which is poor when the block size gets too small.

The second task to be solved for visual servoing is the feedback control for high precision camera pointing. The pointing control is commonly based on two possible fine/coarse pointing principles. The first one uses a single actuator in a cascaded control loop with a high bandwidth inner loop (velocity or relative position control) and a low

bandwidth outer loop with high accuracy visual feedback signals based on the real-time image motion measurement, e.g. (Ferreira & Fontaine, 2001). The second principle uses two actuators in parallel: a low-bandwidth large stroke (coarse position) actuator serves to move a high-bandwidth short-stroke (fine position) actuator, which results in a dual input–single output (DISO) system (Schroek, Messner, & McNab, 2001). In both cases the challenges for control design come from structural vibrations and noise and computation time delay from the image motion signals. These fine/coarse pointing principles have been applied successfully to optical space systems such as inter-satellite laser communication (Fletcher, Hicks, & Laurent, 1991; Griseri, 2002; Guelman et al., 2004), as well as to low cost aerial imaging systems (Oh & Green, 2004).

The challenges for the *high resolution satellite imaging* application discussed in this paper are determined by low brightness and fast motion of the focal plane image as well as high accuracy requirements for motion correction. The focal plane image moves typically with a velocity of 3450 pixels per second for an Earth observations mission with a ground resolution of 2 m per pixel at a 600 km orbit altitude. Without motion compensation the exposure time should be limited to 0.2 ms to prevent image blurring. Such a short exposure will result in a signal to noise ratio below 10 dB (for an aperture diameter of 150 mm) — see Fig. 1.

An innovative concept of an opto-mechatronic stabilization assembly for high precision positioning of the focal plane assembly has been proposed by Janschek and Tchernykh (2001). The proposed assembly consists of a high-speed onboard optical processor for in situ real-time image motion measurement and a single 2-axis piezo-drive assembly in a cascaded control loop configuration. This visual servoing concept allows minimizing the size of the optics and the sensitivity to attitude disturbances and it shows a high robustness to image noise. One of the most critical aspects for the motion compensation is the performance of the in situ image motion measurement

and tracking in terms of high computational speed and high measurement accuracy. The demanding real-time requirements are covered by the use of a compact embedded optical correlator. This innovative and not yet commercially available technology allows the use of large image blocks up to 256×256 pixels, which ensures the required high accuracy for motion measurement combined with a high robustness for dark and fast moving images.

This paper presents new results in terms of a detailed performance analysis of the image motion tracking subsystem and it is organized as follows. After a brief overview of the overall system concept the paper discusses the basic structure and main operations of the opto-mechatronic feedback loop as well as the fundamental principles of the image motion measurement using an optical joint transform correlator. The main part of the paper is focusing on the performance analysis of the image motion measurement subsystem, as those performances are determining fundamentally the achievable image stabilization quality. The image motion tracking error analysis is based on the statistical analysis of a broad scope of simulation and flight data and provides justified performance figures compared to previous publications. Based on these performance figures the achievable system end-to-end capabilities of image motion compensation are demonstrated by simulation results. Complementary results from laboratory tests with a functional breadboard of the opto-mechatronic assembly conclude the paper and prove the feasibility of the proposed concept.

2. System concept

A system layout of the opto-mechatronic stabilization assembly is shown in Fig. 2. The focal plane motion with respect to ground is measured by an *auxiliary matrix* (area) *image sensor* and an *optical correlator*. The auxiliary sensor is installed in the focal plane of the imaging system which produces a sequence of images. These sequences are used for the image motion measurement on the basis of a 2-dimensional spatial correlation of sequential image pairs. The correlation approach results in subpixel accuracy for the shift vector determination, it is independent from specific image textures and it is extremely robust against image noise. The demanding computational requirements for the real-time 2D-correlation are covered by an embedded optical correlation processor (Joint Transform type).

A mechanical compensation of the disturbing focal plane motion is performed by a 2-axis moving platform which can be driven by piezo actuators or piezo motors.

Direct piezo-electric actuators use piezo-electric forces to convert an electrical signal into a proportional displacement of an output element. They have large bandwidth (up to kHz), but small stroke (typically within 0.1–0.2 mm) therefore they can be used only to compensate the image motion disturbances, caused by the attitude instabilities and vibrations (normally these disturbances have relatively

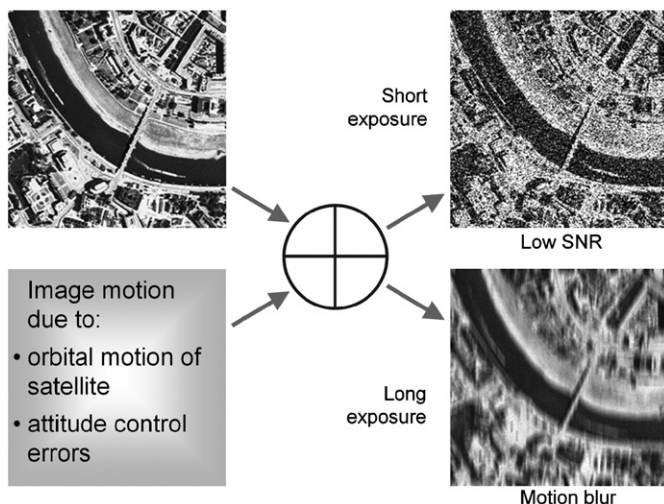


Fig. 1. Camera imaging disturbances.

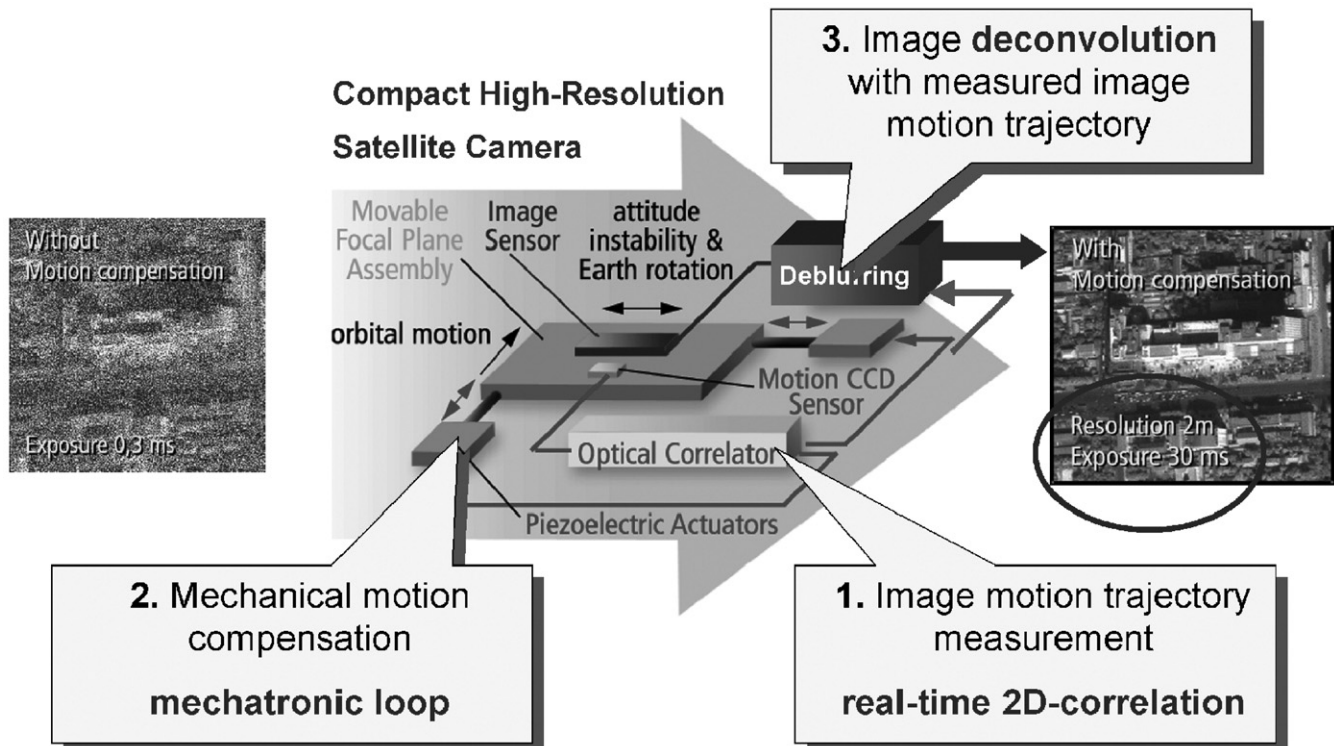


Fig. 2. Opto-mechatronic system concept.

small amplitude). Image motion, caused by orbital motion of the satellite, can be in this case compensated by electronic TDI.

Piezo motors use a combination of piezo-electric and friction forces to generate a progressive motion of an output element. They have much larger stroke (few tens of millimeters is possible also with compact devices), so they can be used for total compensation of all focal plane image motion (especially if the spectrum of such motion is limited).

Both direct piezo actuators and piezo motors are currently available for space applications, e.g. XYZ position stage with piezo actuators onboard ROSETTA probe (Le Letty et al., 2001); linear piezo motor developed and space qualified by CEDRAT Technologies (CEDRAT, 2005).

Feedback signals derived from in-situ image motion measurements allow precise motion compensation. Residual image disturbances can be compensated by image deconvolution using the measured focal plane motion trajectory (Janschek, Tchernykh, & Dyblenko, 2005).

The high speed measurement of the image motion is fundamental for the proposed application: to minimize the delay in feedback loop, the exposure time for the motion sensor should be very short, which results in extremely low SNR of the motion sensor images (down to 0 dB).

As a result of the proposed image motion compensation, a camera with a ground resolution of 2 m per pixel (from 400 km orbit) can be realized within an envelope of $130 \times 130 \times 320$ mm and a mass within 4 kg (Fig. 3). Such

Compact High-Resolution Satellite Camera

- robust to residual attitude motion (e.g. small sat)
- shoe-box size (130 x 130 x 320 mm)
- mass: 4.0 kg
- power consumption: 5 W during imaging
- optics: Maksutov-Cassegrain telescope
- focal length: 1000 mm
- aperture: 106 mm
- ground resolution: 2.0 m per pixel (from 400 km orbit)

Fig. 3. High resolution camera specification.

a camera can be easily installed onboard small satellites with moderate attitude stability or as a secondary payload on non-remote sensing platforms (low Earth orbit communication satellites, space station).

3. Opto-mechatronic feedback loop

The general control loop structure is shown in Fig. 4.

The inner loop controls the velocity V_{pl} of the movable focal plane platform with respect to the satellite frame. V_{pl} is measured by a conventional displacement sensor and is

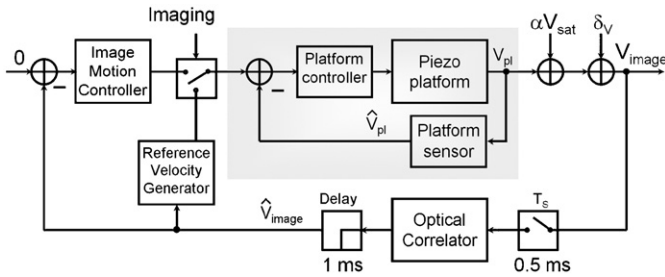


Fig. 4. Control loop structure.

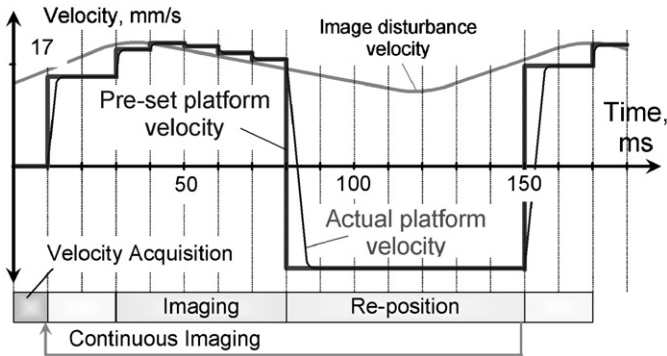


Fig. 5. Velocity profiles.

maintained equal to the required commanded value from the outer loop. The inner loop is closed continuously and has a bandwidth of a few hundred hertz.

The outer loop controls the velocity of the image motion with respect to the platform V_{im} . This velocity should be minimized during imaging to prevent the image blur. For this, the disturbing image motion due to satellite motion (αV_{sat}) and due to attitude control errors (δv) should be compensated. The value of V_{im} is measured by the optical correlator and applied to the image motion controller. The controller produces the value of the platform velocity, required for compensation. This value is entered as command into the inner loop.

The outer loop is closed only during imaging phases. To maintain high stability in presence of measurement delay (1 ms), the bandwidth of the outer loop is limited to few tens Hz, so inner and outer loops are well decoupled in frequency domain. This limited bandwidth of the outer loop is sufficient for accurate image motion compensation, as the spectrum of the image motion disturbances due to satellite motion αV_{sat} and attitude control errors δv are well limited by typically few hertz.

The velocity profiles (with respect to the satellite frame) during the main stages of operation are sketched in Fig. 5.

After activation of the system the optical correlator measures the image velocity with respect to the platform (velocity acquisition interval in Fig. 5). During the synchronization interval the outer loop controller uses this data to produce the command value for the platform velocity, required to compensate the image motion, and sends this value to the inner loop controller. Within 10 ms

the platform accelerates to the required velocity, then the residual image motion is checked by the optical correlator and (if necessary) corresponding corrections of the pre-set platform velocity are performed.

When synchronization is completed, the system enters the image following mode: the platform follows the motion of the image and the resulting image velocity with respect to the platform is close to zero. During this phase the image can be exposed without motion blur effect and distortions. The duration of the image following mode for the given reference mission parameters and maximum travel distance of the movable platform of 2 mm can be up to 100 ms.

After finishing the image exposure, the platform needs to be repositioned for the next imaging cycle. This is done by applying an appropriate fixed negative value to the command input of the inner control loop. To prevent an error accumulation, repositioning is terminated by a limit switch.

The value of platform velocity at the end of the imaging cycle can be used as initial velocity estimation for the next cycle. Such a procedure will eliminate the need for the velocity acquisition interval and thus improves the imaging repetition frequency.

In particular beneficial for this application is the measurement robustness to image noise. To provide the required bandwidth of the visual feedback, the images from the auxiliary image sensor will be taken with a very short exposure and thus will have only a low signal-to-noise ratio.

4. Image motion measurement by 2D-correlation

The image motion is measured by 2D correlation of the sequential images (Fig. 6) and post-processing of the correlation image. The so-called joint transform correlation scheme is used to minimize the overall computational effort. It makes use of two subsequent 2D-Fourier transforms without using phase information (Fig. 7).

As a result, the vector of mutual shift of the sequential images can be determined. High redundancy of the correlation procedure permits to obtain subpixel accuracy of shift determination even for low SNR dark images. It has, however, one significant drawback — a huge amount

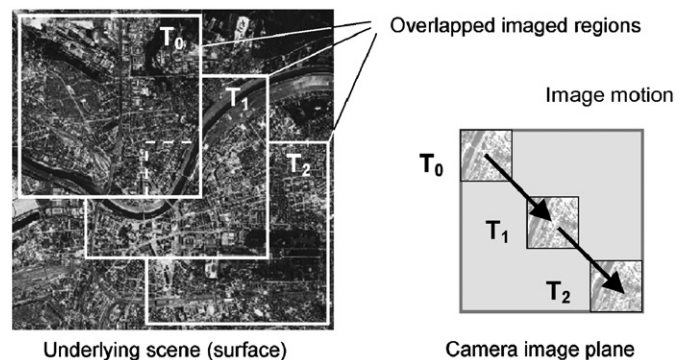


Fig. 6. Image motion tracking.

of calculations, required to perform the 2D correlation digitally. To overcome this limitation, fast optical image processing techniques can be applied (Goodman, 1968; Jutamulia, 1992; Stark, 1982).

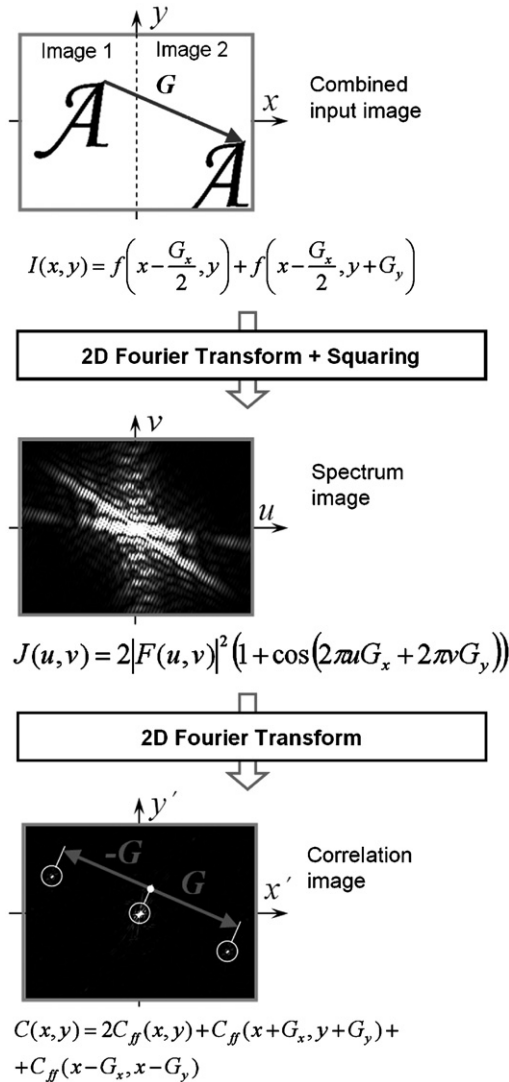


Fig. 7. Principle of joint transform correlation.

A *Joint Transform Optical Correlator* (JTC) is an optoelectronic device, capable of the fast determination of the shift between two images with overlapping image contents. JTC includes two identical optoelectronic modules — Optical Fourier Processors (OFP) — as sketched in Fig. 8.

Two digital input images (current and reference images) are entered into the optical system of the first OFP by a transparent *spatial light modulator* (SLM). After a first optical Fourier transformation, the joint power spectrum (JPS) is read by the CCD image sensor and loaded to the SLM of the second OFP.

A second optical Fourier transformation forms the resulting correlation image. If both input images contain overlapping regions, the correlation image will contain two symmetric correlation peaks. The shift of these correlation peaks relative to optical axis corresponds to the shift between the current and reference input images (Jutamulia, 1992).

The position of peaks on the correlation image and the corresponding shift value can be measured with sub-pixel accuracy using standard digital algorithms for centre of mass calculation (Fisher & Naidu, 1996). Optical processing thus allows a unique real time processing of high frame rate video streams.

This advanced technology (which is not yet commercially available today) and its applications are studied during last years at the Institute of Automation of the Technische Universität Dresden. Different hardware models have been manufactured, e.g. under European Space Agency (ESA) contract.

Due to special design solutions the devices are very robust to mechanical loads and do not require precise assembling and adjustment (Tchernykh, Janschek, & Dyblenko, 2000). Recent airborne test flight results showed very promising performances (Tchernykh, Dyblenko, Janschek, Göhler, & Harnisch, 2002).

Optical processing technology allows reaching high correlations rate also with considerably large correlated fragments. Correlation of large fragments ensures high accuracy of image motion measurements also for extremely noisy images with SNR less then 0 dB. With currently

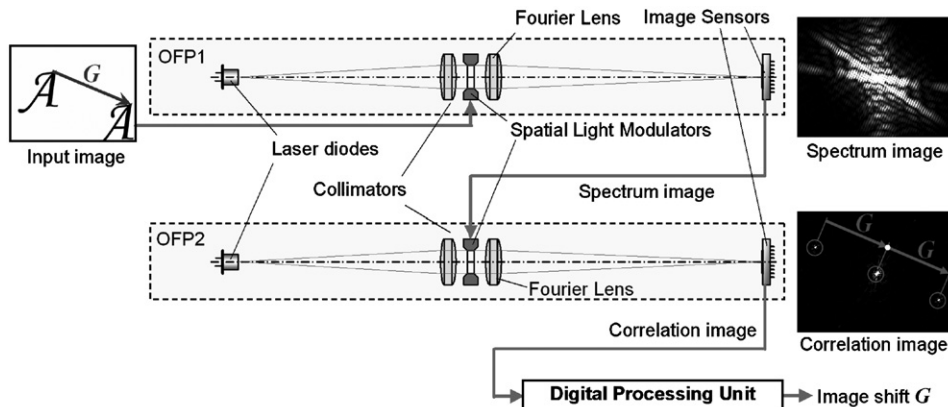


Fig. 8. Joint Transform Optical Correlator (JTC)

available optoelectronic components following performances of an optical correlator can be achieved:

- correlation rate — 2000 correlations/s with image fragments 256×256 pixels;
- processing delay — 1 ms;
- RMS error of image motion determination — within 0.05 pixels for most of the textures.

With customized components these performances can be even further improved.

The ability to process very noisy images makes the optical correlator particularly suitable for the determination of the fast motion of dark images in the focal plane of a compact satellite camera. The achievable high correlation rate makes it also suitable for mobile robotics applications (image motion analysis for visual laboratory navigation, collision avoidance, visual servoing, etc.).

5. Image motion tracking error analysis

5.1. Error modeling

The image motion tracking provides the vital feedback signal for high precision compensation of orbital motion and correction of motion disturbances of the primary image sensor. For this purpose a detailed analysis of the expected accuracy and main error characteristic of these measurements in terms of an error model is essential.

Image motion tracking consists of a number of image motion measurements. The tracking algorithm determines the positions of a moving image block on the image sensor at certain time moments. Single image motion measurement \mathbf{s}_j is performed by extrapolation (prediction) \mathbf{p}_j of the image movement from the previous position to this time moment and a subsequent correction \mathbf{d}_j of the prediction error by measurement of the shift between the previous reference image and the image taken from the predicted position (Fig. 9).

On each tracking step the measured image motion vector $\hat{\mathbf{s}}_j$ is determined with some measurement error

$$\hat{\mathbf{s}}_j = \mathbf{s}_j + \mathbf{e}_j,$$

where \mathbf{s}_j is the true image motion vector.

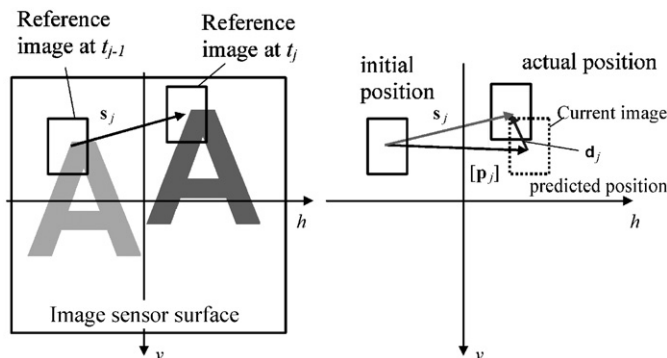


Fig. 9. Prediction and correction of reference image motion.

The image motion measurement error \mathbf{e}_j includes:

- error of pure translational image motion measurement;
- error caused by geometrical distortions of the image;
- error caused by noise of the camera sensor.

As shown by (Dyblenko, 2004) the error caused by geometrical image distortions can be kept sufficiently small and corrected to a negligible level. The influence of imaging noise becomes important only at a rather high noise level and under real conditions, it has a negligible effect on the image shift measurement accuracy.

The most important contributor however is the error of pure translational image shift measurement, which is caused by the algorithm for determination of the correlation peak position.

5.2. Error characteristics of translational image shift measurement

This defines the error of image motion measurement produced by the image tracker based on the joint transform correlation algorithm for matching of two images. The correlated images are considered to be different by the image shift only. It is supposed that the acquired surface image information has spatial frequencies below half of sampling frequency of the image sensor and therefore the images are obtained without aliasing effects.

On each tracking step for each image block one reference and one current image block are obtained by the image sensor at time moments t_{j-1} and t_j , respectively (Fig. 9).

The true vector of reference image motion \mathbf{s}_j is determined by the procedure of prediction/correction as

$$\mathbf{s}_j = [\mathbf{p}_j] - \mathbf{d}_j, \tag{1}$$

where \mathbf{p}_j is the predicted image motion vector, \mathbf{d}_j the actual shift vector between predicted and actual image positions, $[\dots]$ the rounding operation.

The predicted motion vector \mathbf{p}_j is calculated using a model of image motion, which describes the relationship between positions of the image blocks and measured data about position and orientation of the camera and a priori data about planet shape and rotation. Then this vector is rounded to obtain the location of the current image.

In the general the vector

$$\mathbf{p}_j = F(\mathbf{D}_j) \tag{2}$$

depends on a set of parameters \mathbf{D}_j , e.g. the focal vector defining the location of reference image block at acquisition time t_{j-1} , satellite position vectors and Roll–Pitch–Yaw attitude vectors of the camera at times t_{j-1} and t_j , as well as on a priori rotational and geometrical planet shape models used by the system during operation (with index j means, that the data are defined at time t_j).

In practice, these parameters are known with some error,

$$\Delta\mathbf{D}_j = \mathbf{D}_j - \mathbf{D}_j^0,$$

where \mathbf{D}_j^0 represents the true values (i.e. position, attitude a priori model data).

The error $\Delta\mathbf{D}_j$ results in an error of image motion prediction, which is by definition

$$\mathbf{d}'_j = \mathbf{p}_j - \mathbf{s}_j = G(\Delta\mathbf{D}_j), \quad (3)$$

where $G(\Delta\mathbf{D}_j)$ is an error function, which can be obtained by error analysis of Eq. (2).

For a smooth and continuous distribution of \mathbf{p}_j , the rounding operation of \mathbf{p}_j can be approximated as

$$[\mathbf{p}_j] \approx \mathbf{p}_j + U(-0.5 \dots + 0.5), \quad (4)$$

where $U(-0.5 \dots + 0.5)$ is uniformly distributed random variable in the range $-0.5 \dots + 0.5$.

Taking into account Eqs. (1), (3) and (4),

$$\mathbf{d}_j \approx \mathbf{d}'_j + U(-0.5 \dots + 0.5)$$

or

$$\mathbf{d}_j \approx G(\Delta\mathbf{D}_j) + U(-0.5 \dots + 0.5). \quad (5)$$

Eq. (5) shows a strong correlation between the measured image shift \mathbf{d}_j and uncertainties in position, attitude and a priori model data used for the prediction.

Image matching gives the measured image shift $\hat{\mathbf{d}}_j$, which differs from the actual value by some error ε_j and

$$\hat{\mathbf{d}}_j = \mathbf{d}_j + \varepsilon_j. \quad (6)$$

Taking into account Eqs. (1) and (6) the measured image motion vector is defined as

$$\hat{\mathbf{s}}_j = [\mathbf{p}_j] - \hat{\mathbf{d}}_j = \mathbf{s}_j + \varepsilon_j.$$

As the image shift measurement is based on the determination of correlation peak position, the error of image shift and image motion measurement ε_j becomes equal to the error of the determination of the correlation peak position.

It can be shown that for mutually shifted images the tip of correlation peak differs from the centre of mass of the correlation function, which is actually used to determine with sub-pixel accuracy (Fisher & Naidu, 1996) the location of the correlation peak (Dyblenko, 2004).

The problem of a precise analytical relation between the image shift measurement error and image shift and image content has not yet been solved. In Dyblenko (2004) a stochastic error model is studied which investigates a variety of possible image models represented by random processes with different spectral densities. For real image textures the spatial spectral components decrease for higher spatial frequencies.

The 2D-error of single shift measurement is defined according to Eq. (6) as

$$\boldsymbol{\varepsilon} = \hat{\mathbf{d}} - \mathbf{d} = \begin{pmatrix} \varepsilon_h \\ \varepsilon_v \end{pmatrix},$$

where subscripts h and v show horizontal and vertical error components, respectively.

Series of simulation experiments was performed for different random models of images. For each model statistical properties of $\boldsymbol{\varepsilon}$ were estimated for different image shift values \mathbf{d} (whole numbers of pixels). The results of the simulations are shown in Fig. 10. The standard deviations were estimated by root-mean-square error (RMS) calculated for the error samples.

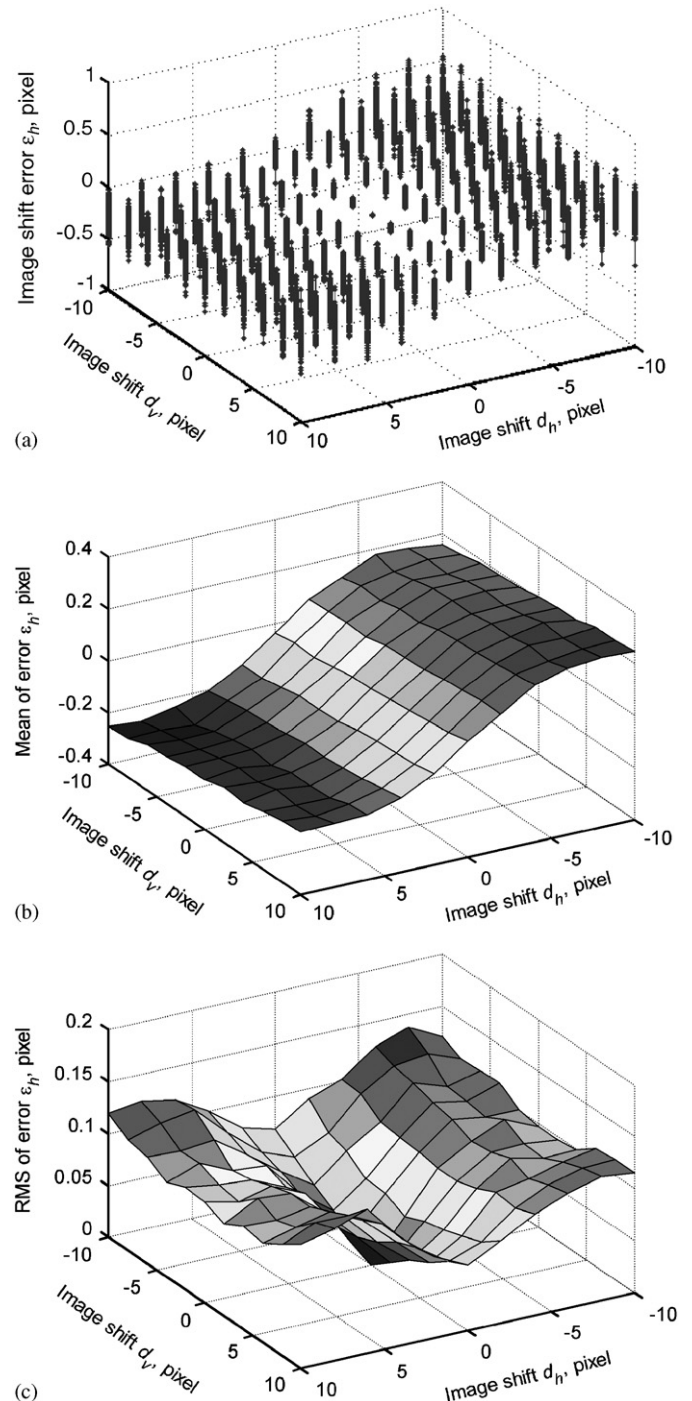


Fig. 10. Simulation results of image shift measurement: (a) values of horizontal image shift measurement error for different image shifts; (b) estimated mean values of horizontal error for different image shifts; (c) estimated standard deviations of horizontal error for different image shifts.

The number of simulation for each value of \mathbf{d} was 200. The confidence interval for the estimates of standard deviation can be roughly estimated as $\pm 6\%$ at a confidence level of 0.9. The confidence interval for estimates of mean for large \mathbf{d} can be roughly given as $[-0.02\dots +0.02]$ at a confidence level of 0.9. It decreases for smaller \mathbf{d} due to the decrease of the standard deviation.

Generally, each error component can be represented by a non-linear regression model

$$\boldsymbol{\varepsilon} = g(\mathbf{d}) + \boldsymbol{\eta},$$

where the regression function $g(\mathbf{d})$ is by definition $E(\boldsymbol{\varepsilon}|\mathbf{d})$, and $\boldsymbol{\eta}$ is a residual term.

Obviously, $g(\mathbf{d})$ is a function, which should depend on image model type. The residual term $\boldsymbol{\eta}$ represents a random variable, which has a distribution with zero mean and variance $\sigma_{\boldsymbol{\eta}}^2(\mathbf{d})$ depending on the image shift value and image model type. The random variable $\boldsymbol{\eta}$ is uncorrelated with \mathbf{d} .

For a small range of image shift (about ± 5 pixels) a linear regression model can be used,

$$g(\mathbf{d}) \approx \mathbf{K} \cdot \mathbf{d} = \begin{pmatrix} k_{11} & k_{12} \\ k_{21} & k_{22} \end{pmatrix} \cdot \begin{pmatrix} d_h \\ d_v \end{pmatrix},$$

$$\sigma_{\boldsymbol{\eta}}(\mathbf{d}) \approx \mathbf{W} \cdot |\mathbf{d}| = \begin{pmatrix} w_{11} & w_{12} \\ w_{21} & w_{22} \end{pmatrix} \cdot \begin{pmatrix} |d_h| \\ |d_v| \end{pmatrix}.$$

It can be seen, that $k_{11} \gg k_{12}$, $k_{22} \gg k_{21}$ and the non-diagonal elements k_{12} and k_{21} are close to zero. The mean value for an error component is sufficiently accurate determined by the corresponding component of image shift, whereas the standard deviation value for an error component residual is determined by both components of the image shift vector.

The resulting distribution of $\boldsymbol{\eta}$ is rather close to Gaussian, as can be seen by histograms in Fig. 11.

As a result the stochastic model of image shift measurement for small ranges of image shift \mathbf{d} and a

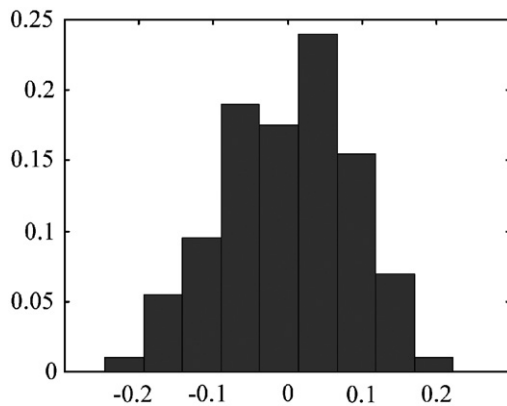


Fig. 11. Normalized histograms for random parts of the image shift horizontal measurement error η_h .

specific image model can be given as

$$\boldsymbol{\varepsilon}(\mathbf{d}; \mathbf{K}, \mathbf{W}) \approx \mathbf{K}\mathbf{d} + \boldsymbol{\eta},$$

where $\boldsymbol{\eta}$ is a random vector with distribution of each component close to Gaussian and variance $\sigma_{\boldsymbol{\eta}}^2(\mathbf{d}) \approx (\mathbf{W} \cdot |\mathbf{d}|)^2$. Matrices \mathbf{K} and \mathbf{W} are specific for a certain image model.

For larger image shift ranges the functions $g(\mathbf{d})$ and $\sigma_{\boldsymbol{\eta}}(\mathbf{d})$ can be approximated piecewise by higher order polynomials.

Different measurements of image shift may have independent errors, if they are done for images with partial overlapping. The critical overlapping value changes for images with generally different spectra and is normally above 80%.

The measurement error is resulting from the non-symmetrical change of the correlation peak shape at some image shift. The convolution theorem shows, that the shape of the correlation function around a correlation peak directly depends on the joint power spectrum of the correlated images. The error of the peak position determination is the same for identical image pairs with correspondingly identical joint power spectra. It has been shown by Dyblenko (2004) that matching of image pairs with generally similar joint power spectra will result in a similar shape of the correlation peaks and, therefore in a similar magnitude of the measurement error.

To find a distribution of the error components for a specified image model a series of independent images from the given model were generated. Then from each test image one reference and one current image were extracted so that they became shifted by a value \mathbf{d} . For each pair of reference and current images a value for image shift vector \mathbf{d} was chosen as uniformly distributed random vector with independent components in the range $[-15\dots +15]$ whole pixels.

Fig. 12a shows spectral densities of the random image models used in the experiment. The error model parameters are presented versus the cut frequency of the model spectral density at a level of 10%. The estimated standard deviation of the random residual $\boldsymbol{\eta}$ is represented by the average value for root-mean-square errors for image shifts in the range of ± 5 pixels and is shown for the horizontal and vertical error components separately in Fig. 12b.

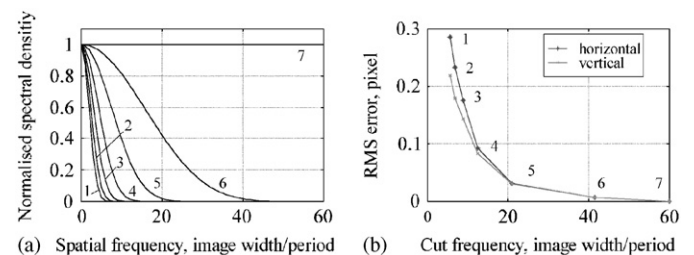


Fig. 12. Parameters of image shift measurement error estimated for different random image models: (a) spectral densities of test image models; (b) estimated standard deviations of error components.

There is a clearly observable monotone dependency between the width of the spectral density of the random image model and the parameters of the image shift measurement error. Matching of more smoothed images produces larger error. It is important, that similar spectra represent similar error parameters. For close spectral densities 1 and 2 the difference of the standard deviation is rather small (14–18%), whereas for wide apart spectral densities 5 and 6 the difference is 80%, which is about 4 times larger.

The range of image shifts for which a linear error model can be approximated is larger for more smoothed images. In the experiment carried out, an interval of $[\pm 1 \dots \pm 10]$ pixels has been estimated.

It can be assumed, that the comparison of the power spectrum of a given real image with spectral densities of reference image models can allow the estimation of parameters of the image shift measurement error.

Decreasing the size of the image blocks can reduce the calculation time but results in reduced accuracy. The measurement error is increased due to larger non-symmetric distortions of the correlation peak. Fig. 13 shows estimated results for different image size. Image texture model was of type 4 (according to spectral density in Fig. 12). The range of image shift is ± 4 pixels.

It can be concluded, that for different image size the residual error η changes approximately inverse to the image area, whereas the time for calculation of the correlation function is proportionally to the image area.

5.3. Tracking robustness to image content

The robustness of the shift vector determination with respect to different image texture has been analyzed by a variety of different images. Fig. 14 shows such a test image with a ground resolution of 0.25 m per pixel from an aerial test campaign of High Resolution Stereo Camera HRSC-AX and processed at DLR, Institut für Planetenforschung. The image contains areas with different texture, what makes it possible to test the system operation with different image content. For the 2D correlation all fragments of the base image were re-sampled to a resolution of 0.75 m per

pixel. Subpixel image motion has been simulated by shifting (also subpixel) of the base image fragments before re-sampling. The motion blur has been simulated in Fourier domain, by multiplication with Fourier transform of the motion vector.

The image block size for image motion tracking was chosen 128×128 pixel with grey scale 0...255 and random additive image noise 20 grey scale bit (1σ).

Fig. 15 shows the 2D-distribution of the image shift estimation error (sum of bias and random errors 1σ). In Fig. 16 the error distribution pattern is superimposed onto the test image. The error varies from 0.013 pixels for areas with strong texture up to 0.104 pixels for low texture areas. The average error value for the whole test image was 0.027 pixels.



Fig. 14. Test image.

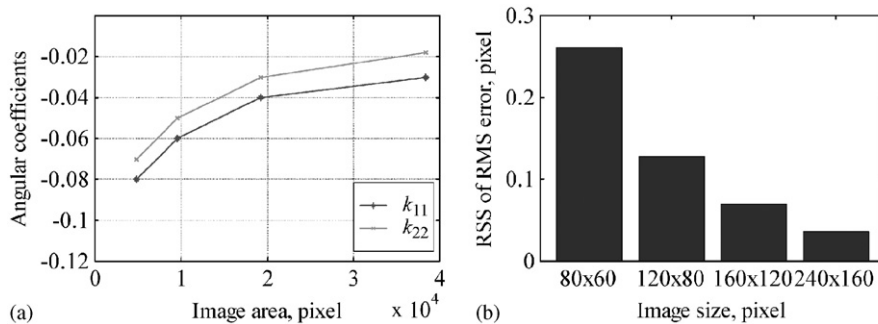


Fig. 13. Parameters of image shift measurement error versus image size: (a) estimated parameters of error linear regression k_{11} and k_{22} ; (b) estimated standard deviations of error components.

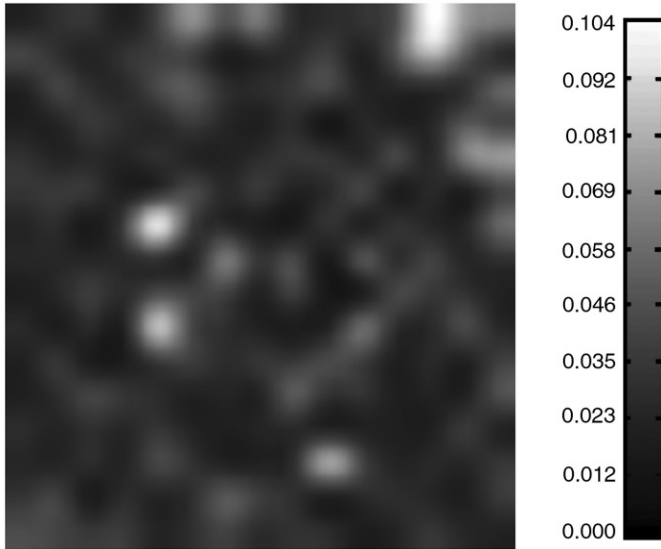


Fig. 15. 2D-distribution of the image shift estimation error (pixels).

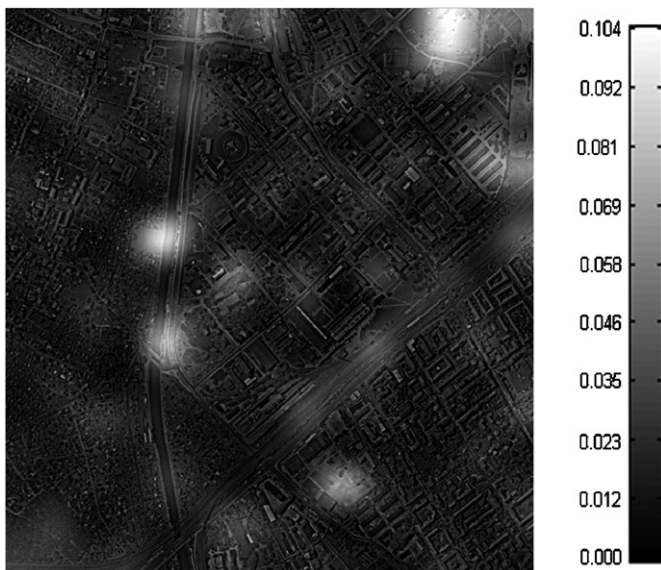


Fig. 16. 2D-distribution of the image shift estimation error superimposed on the test image.

5.4. Results of the testing of hardware optical correlator model

The tests have been performed with the hardware model of an embedded optical correlator (Fig. 17), manufactured within the frame of an ESA-funded project (Tchernykh et al., 2002).

The model is based on the scheme of the Joint Transform Optical Correlator and includes two identical optical Fourier processors. It has been designed for the real time processing of the video streams from two standard video cameras ($2 \times 30 = 60$ frames per second). To cope with the limited project funding and to save development time, the

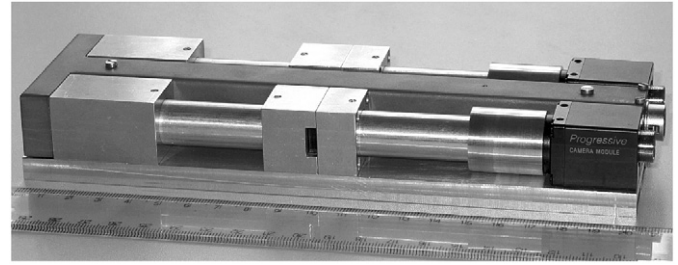


Fig. 17. Optical processor model.

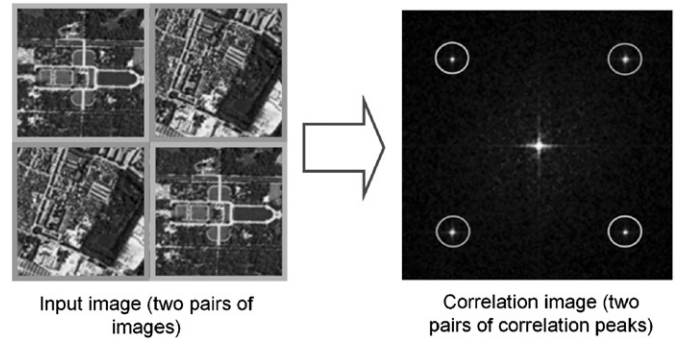


Fig. 18. Simultaneous processing of two image pairs.

model uses standard video cameras as the image sensors within each optical Fourier processor. This limits the image processing rate to 30 optical Fourier transforms per second or 30 correlations per second with two optical Fourier processors (one correlation requires two Fourier transforms). To provide the required 60 correlations per second the image processing rate for each of them has been doubled by simultaneous processing of two image pairs (Fig. 18).

Each pair of input images produces a pair of correlation peaks, which are then processed separately and two image shifts are determined.

As a result of these test the RMS error of image shift determination has been determined to be within 0.15 pixels for most of the image textures (correlated fragments 120×128 pixels). The difference compared with the results of the software simulation (0.013 ... 0.103 pixels, depending on image texture — see previous chapter) is caused mainly by simultaneous processing of two image pairs (appeared to cause strong degradation of correlation peaks magnitude and therefore significant increase of errors) and using the centre-of-mass finding algorithm for correlation peak position determination (features significant increase of errors if the correlated images are shifted by fractional number of pixels and if the shape of the peaks is unsymmetrical). With single-channel correlation, using the advanced algorithms for peaks positions determination and increasing the size of correlated fragments to 256×256 pixels, the error of image shift determination can be kept within 0.05 pixels for most of the image textures.

6. End-to-end image motion compensation simulation results

Fig. 19 shows simulated images for the given reference mission parameters (2 m ground resolution per pixel from 600 km orbit), taken in presence of attitude disturbances, which are typical for a moderately stabilized satellite (residual angular velocity w.r.t. nadir of 0.02°/s).

The noise figures were calculated for limited aperture optics (aperture diameter of 150 mm), with average detector characteristics and observation conditions.

Top image in Fig. 19 corresponds to the case with no image motion compensation. In this case the exposure time should be extremely short to prevent motion blur. For given simulation conditions exposure interval should be reduced to 0.15 ms to keep the image shift within 0.5 pixels. Such a short exposure, however, results in very low signal-to-noise ratio (6 dB), which makes the image practically unusable.

Middle image in Fig. 19 simulates the effect of electronic TDI with 64 steps. Compensation of the image shift due to the orbital motion allows to increase the exposure time up to 19 ms and to improve the SNR value up to 30 dB.

However, electronic TDI does not compensate the image motion disturbances, caused by the attitude instabilities and vibrations. For the given simulation conditions, this results in the residual image shift of 2 pixels, which makes the image blurred and causes significant resolution degradation.

Bottom image in Fig. 19 simulates the effect of the proposed opto-mechatronic image motion compensation. The exposure can be increased up to 50 ms, what improves the SNR value up to 40 dB. The motion tracking errors analysis in the previous chapter shows, that the image motion determination errors can be kept below 0.05 pixels using an optical correlator with image correlation fragments of 256 × 256 pixels. With such a measurement performance it is possible to compensate all components of the image motion within the opto-mechatronic control bandwidth with a residual error below 0.1 ... 0.2 pixels, what is sufficient to obtain a perfectly sharp image.

The simulation results clearly indicate the advantages of the proposed system for image motion compensation: its application makes it possible to produce high quality images even with moderate attitude stability of the satellite and a limited aperture of the optical system.

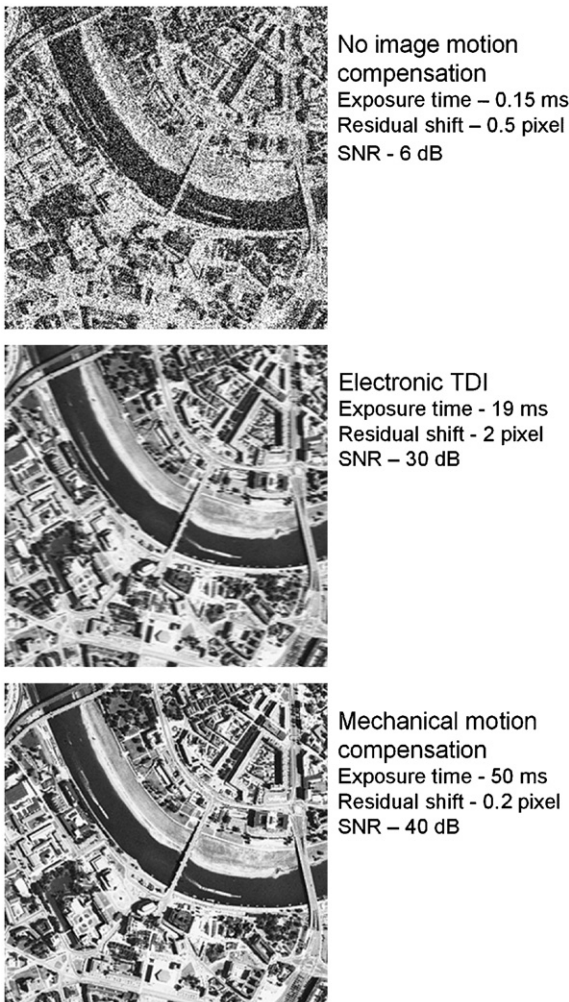


Fig. 19. Image correction—simulation results.

7. Functional hardware-in-the-loop tests

A camera breadboard assembly has been developed for a functional laboratory demonstration of the proposed opto-mechatronic concept (see Fig. 20).

It consists of a piezo platform (motorized stage) of the type L-114 from Micro Pulse Systems (www.micropulse-systems.com) and a standard CCD camera as auxiliary matrix sensor.

The piezo platform L-114 is a compact linear stage that can be stacked to form X–Y stages. It is driven by two piezo actuators and features a no-load speed of 50 mm/s, total travel distance of 13 mm and minimal translation resolution of 0.1 μm. Overall dimensions of the stage are 48 × 48 × 14 mm, mass — 90 g.

A complete hardware-in-the-loop (HWIL) test bench has been built-up using the xPC-Target environment as implementation platform for the control algorithms (see

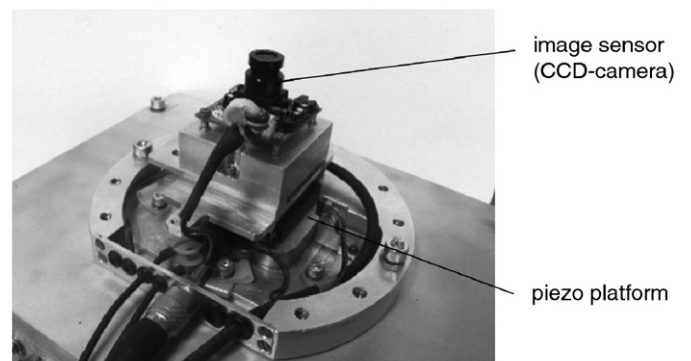


Fig. 20. Camera laboratory breadboard.

Figs. 21 and 22). The camera motion is simulated by a 5-DOF industrial robot, where representative trajectories can be realized properly.

Preliminary HWIL test results at functional level are shown in Figs. 23 and 24. These tests show the principal closed loop operation at the first integration level, with the 2D correlation performed by software. Currently the

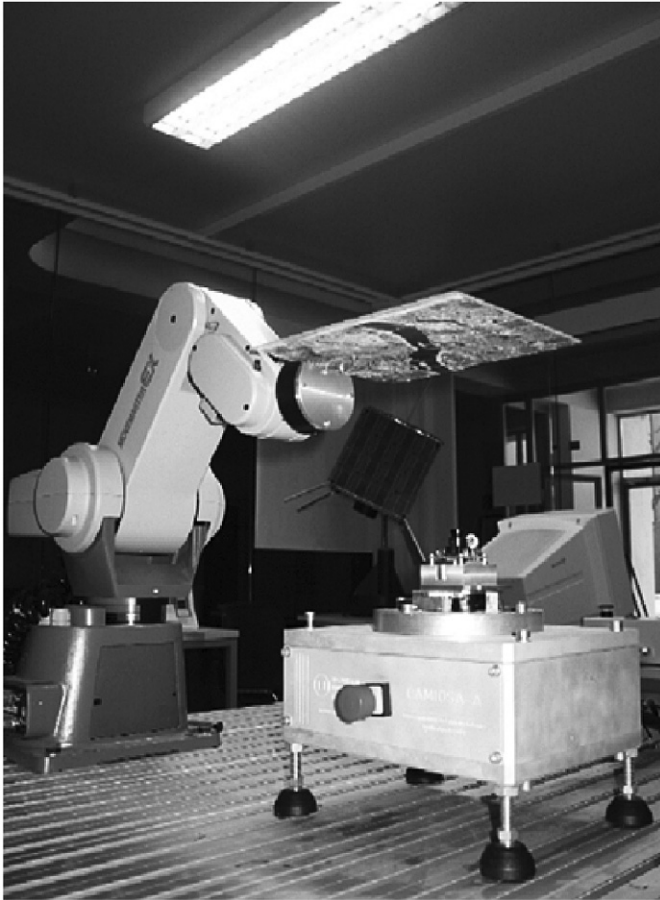


Fig. 21. HWIL test bench.

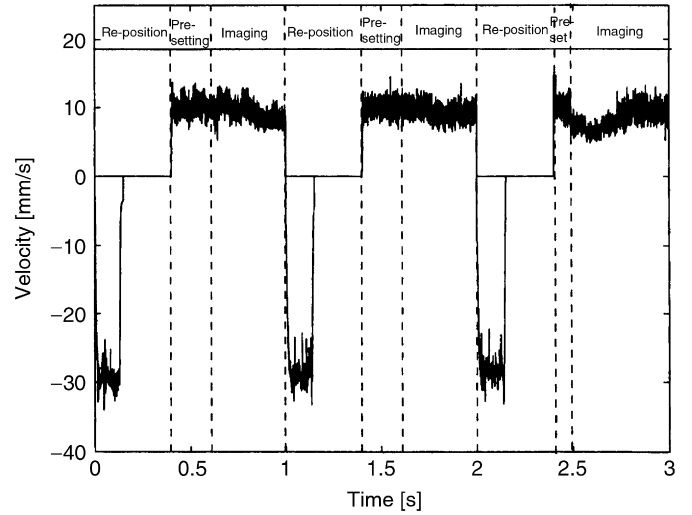


Fig. 23. HWIL test result: platform motion.

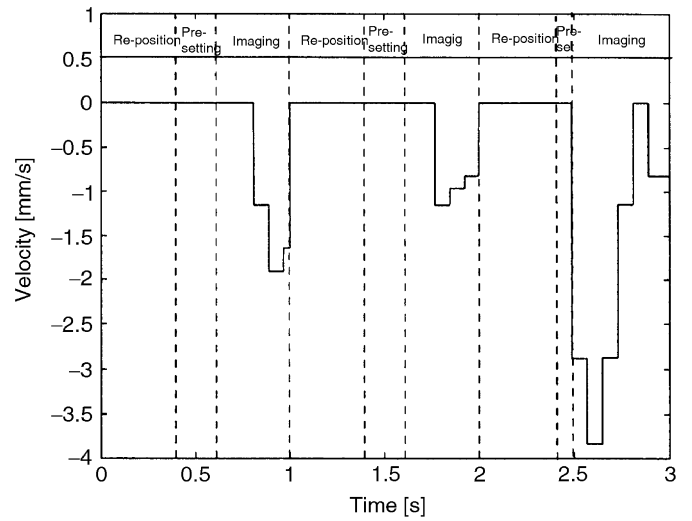


Fig. 24. HWIL test result: image motion measurement by 2D-correlation.

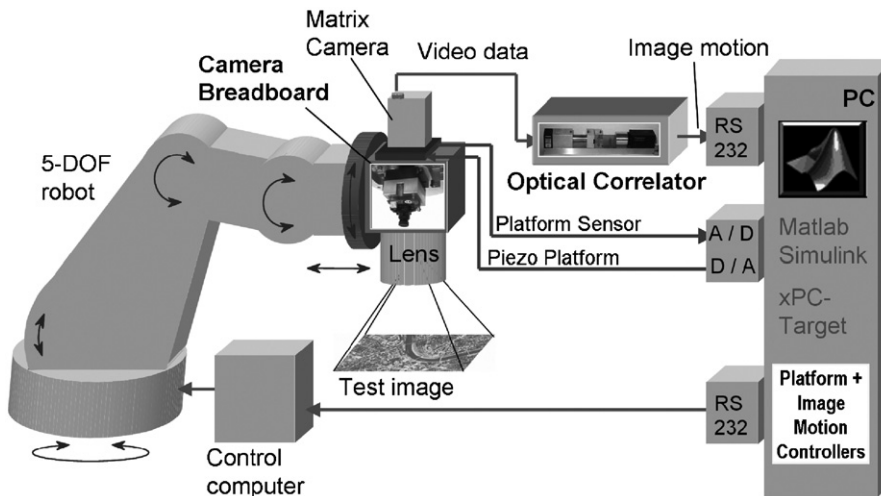


Fig. 22. HWIL test configuration.

optical correlator hardware is being integrated in the loop, which will allow more advanced performance tests under real-time conditions.

8. Conclusions

A previously proposed system concept for an optomechatronic compensation of the image motion in the focal plane of a high resolution satellite camera has been justified by a detailed performance assessment. The optomechatronic system includes an image motion sensor and an embedded optical correlator for precise measurement of the motion of dark and fast moving images. The detailed error analysis of the motion measurement subsystem is based on a software model of the Joint Transform optical correlator and it shows a clear decoupling of the orthogonal image axes and gives detailed figures of the dependencies of the measurement accuracy on image spectral densities and image size. The robustness to different image textures is shown for a set of aerial test images. Preliminary hardware-in-the loop test results with a laboratory functional breadboard model prove the feasibility of the proposed concept. The implementation of the proposed imaging system provides an increase of the quality of the obtained images with a simultaneous reduction of the requirements to the optics aperture diameter and attitude stability of the host satellite.

Acknowledgement

The authors gratefully acknowledge the financial support of European Space Agency for considerable parts of the results presented in this paper, the continuous confidence of Dr. Bernd Harnisch (ESA/ESTEC) in the proposed system concept and the valuable comments of the anonymous reviewers of this paper.

References

- Brodsky, R. F. (1992). Defining and sizing space payloads. In R. W. James, & J. L. Wiley (Eds.), *Space mission analysis and design* (2nd ed, pp. 264–265). Torrance, CA: Microcosm, Inc.
- CEDRAT Technologies (2005). Description of Linear Piezoelectric Motor LPM20-3, www.cedrat.com.
- Dial, G. & Grodecki, J. (2002). IKONOS accuracy without ground control. *Proceedings of ISPRS commission I symposium*, Denver, USA, 10–15 November 2002.
- Dyblenko, S. (2004). *Autonomous satellite navigation with image motion analysis using two-dimensional correlation*. Ph.D. Thesis, Technische Universität Dresden.
- Engelsberg, A., & Schmidt, G. (1999). A comparative review of digital image stabilising algorithms for mobile video communications. *IEEE Transactions on Consumer Electronics*, 45(3), 591–597.
- Ferreira, A., & Fontaine, J.-G. (2001). Coarse/fine motion control of a teleoperated autonomous piezoelectric nanopositioner operating under a microscope. *Proceedings IEEE/ASME international conference on advanced intelligent mechatronics*, 2, 1313–1318 8–12 July 2001 vol. 2.
- Fisher, R. B., & Naidu, D. K. (1996). A comparison of algorithms for subpixel peak detection. In J. Sanz (Ed.), *Image Technology, Chapter #889*. Heidelberg: Springer.
- Fletcher, G. D., Hicks, T. R., & Laurent, B. (1991). The SILEX optical interorbit link experiment. *Electronics and Communication Engineering Journal*, 3(6), 273–279.
- Goodman, J. W. (1968). *Introduction to Fourier optics*. New York: McGraw-Hill.
- Griseri, G. (2002). SILEX Pointing Acquisition and Tracking: ground test and flight performances. *Proceedings of the 5th ESA international conference on spacecraft guidance, navigation and control systems* (pp. 385–391). Frascati (Rome), Italy, 22–25 October 2002.
- Guelman, M., Kogan, A., Kazarian, A., Livne, A., Orenstein, M., & Michalik, H. (2004). Acquisition and pointing control for inter-satellite laser communications. *IEEE Transactions on Aerospace and Electronic Systems*, 40(4), 1239–1248.
- Gullu, M. K., & Erturk, S. (2003). Fuzzy image sequence stabilization. *Electronics Letters*, 39(16), 1170–1172.
- Hansen, M., Anandan, P., Dana, K., van der Wal, G., & Burt, P. (1994). Real-time scene stabilization and mosaic construction. *Proceedings of the second IEEE workshop on applications of computer vision* (pp. 54–62), 5–7 December 1994.
- Haworth, C., Peacock, A.M., & Renshaw, D. (2001). Performance of reference block updating techniques when tracking with the block matching algorithm. *Proceedings of the international conference on image processing* (Vol. 1, pp. 365–368), 7–10 October 2001.
- Hutchinson, S., Hager, G. D., & Corke, P. I. (1996). A tutorial on visual servo control. *IEEE Transactions on Robotics and Automation*, 12(5), 651–670.
- Jain, J., & Jain, A. (1981). Displacement measurement and its application in interframe image coding. *IEEE Transactions on Communications*, 29(12), 1799–1808.
- Janschek, K., & Tchernykh, V. (2001). Optical correlator for image motion compensation in the focal plane of a satellite camera. *Space Technology*, 21(4), 127–132.
- Janschek, K., Tchernykh, V., & Dyblenko, S. (2005). Integrated camera motion compensation by real-time image motion tracking and image deconvolution. *Proceedings of the 2005 IEEE/ASME international conference on advanced intelligent mechatronics* (pp. 1437–1444), July 2005.
- Jutamulia, S. (1992). Joint transform correlators and their applications. *Proceedings of the SPIE*, 1812, 233–243.
- Le Letty, R., Barillot, F., Lhermet, N., Claeysen, F., Yorck, M., Gavira Izquierdo, J., et al. (2001). The scanning mechanism for ROSETTA/MIDAS from an engineering model to the flight model. *Proceedings of 9th ESMATS conference* (Vol. ESA SP480, pp. 75–81), Lewen (B), September 2001.
- Magarey, J., & Kingsbury, N. (1998). Motion estimation using a complex-valued wavelet transform. *IEEE Transactions on Signal Processing*, 46(4), 1069–1084.
- Oh, P. Y., & Allen, K. (2001). Visual servoing by partitioning degrees of freedom. *IEEE Transactions on Robotics and Automation*, 17(1), 1–17.
- Oh, P. Y., & Green, W. E. (2004). Mechatronic kite and camera rig to rapidly acquire, process, and distribute aerial images. *IEEE/ASME Transactions on Mechatronics*, 9(4), 671–678.
- Pratt, W. K. (1974). Correlation techniques of image registration. *IEEE Transactions on Aerospace Electronic Systems*, 10, 353–358.
- Ralis, S. J., Vikramaditya, B., & Nelson, B. J. (2000). Micropositioning of a weakly calibrated microassembly system using coarse-to-fine visual servoing strategies. *IEEE Transactions on Electronics Packaging Manufacturing*, 23(2), 123–131.
- Salaün, J.F., Chamontin E., Moreau G., & Hameury, O. (2002). The SPOT 5 AOCS in orbit performances. *Proceedings of the 5th ESA international conference on spacecraft guidance, navigation and control systems* (pp. 377–380), Frascati (Rome), Italy, 22–25 October 2002.
- Schroek, S. J., Messner, W. C., & McNab, R. J. (2001). On compensator design for linear time-invariant dual-input single-output systems. *IEEE/ASME Transactions on Mechatronics*, 6(1), 50–57.
- Stark, H. (Ed.). (1982). *Application of optical Fourier transform*. New York: Academic Press.

- Tchernykh, V., Dyblenko, S., Janschek, K., Göhler, W., & Harnisch, B. (2002). SmartScan—hardware test results for smart opto-electronic image correction for pushbroom cameras. In Barnes, W. L. (Eds.), *Proceedings of the SPIE, earth observing systems VII* (Vol. 4814, pp. 264–272).
- Tchernykh, V., Janschek, K., & Dyblenko, S. (2000). Space application of a self-calibrating optical processor or harsh mechanical environment. *Proceedings of 1st IFAC conference on mechatronic systems—mechatronics 2000* (Vol. 3, pp. 309–314), Darmstadt, Germany, 18–20 September 2000, Pergamon-Elsevier Science.
- Uomori, K., Morimura, A., Ishii, H., Sakaguchi, T., & Kitamura, Y. (1990). Automatic image stabilizing system by full-digital signal processing. *IEEE Transactions on Consumer Electronics*, 36(3), 510–519.
- Weber, T.E., & Hollis, R.L. (1989). A vision based correlator to actively damp vibrations of a coarse-fine manipulator. *Proceedings of the IEEE international conference on robotics and automation*, (Vol.2, pp. 818–825), 14–19 May 1989 .
- Xu, J. B., Po, L. M., & Cheung, C. K. (1999). Adaptive motion tracking block matching algorithms for video coding. *IEEE Transactions on Circuits and Systems for Video Technology*, 9(7), 1025–1029.